

Inelastic processes in collisions of Na(3s,3p) with He at thermal energies

C. Y. Lin*

LERMA, Observatoire de Paris-Site de Meudon, 5 Place Jules Janssen, F-92 195 Meudon Cedex, France

P. C. Stancil

Department of Physics and Astronomy and Center for Simulation Physics, The University of Georgia, Athens, Georgia 30602-2451, USA

H.-P. Liebermann, P. Funke, and R. J. Buenker

Fachbereich C-Mathematik und Naturwissenschaften, Bergische Universität Wuppertal, D-42097 Wuppertal, Germany

(Received 19 September 2008; published 13 November 2008)

Inelastic collisions of sodium due to low-energy helium are investigated using the quantum-mechanical molecular-orbital coupled-channel method. The calculations adopt adiabatic potentials and nonadiabatic radial and rotational couplings obtained with the multireference single- and double-excitation configuration interaction approach. The potentials are fitted to long-range dispersion coefficients and adjusted with a model interaction in the van der Waals well region. Collisional cross sections for energies between 0.001 eV and 10 eV and rate coefficients as a function of temperature between 10 K and 10 000 K are obtained for Na(3p → 3s) quenching and Na(3s → 3p) excitation. The results are relevant to modeling non-LTE effects in Na *D* absorption lines in extrasolar planets and brown dwarfs.

DOI: [10.1103/PhysRevA.78.052706](https://doi.org/10.1103/PhysRevA.78.052706)

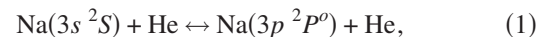
PACS number(s): 34.50.-s

I. INTRODUCTION

In 2001, Charbonneau *et al.* [1] made the first observation of an atmospheric constituent in an extrasolar planet. In a transit observation, they detected sodium absorption in the extrasolar giant planet (EGP) HD 209458b. However, the inferred absorption was only one-half the expected value leading Barman *et al.* [2] to suggest that the electronic states of Na were not in equilibrium. In order to explore the mechanism for the decrease in sodium absorption, well-determined collisional cross section for interactions of Na with the main atmospheric constituents, H₂ and He, are necessary. In particular, electronic excitation processes by neutral species become dominant in cool atmospheric environments due to the small electron abundance.

Although the electronic excitation process of ground-state sodium atoms in collisions with ground-state helium has been investigated in a number of theoretical [3–6] and experimental [7–9] studies, the available data are all above 100 eV. The thermal regime has been relatively unexplored except for studies on fine-structure branching fractions in optical collisions [10] and collisional broadening of Na resonance lines [11]. To shed further light on this problem, we apply the quantum-mechanical molecular-orbital coupled-channel (MOCC) method, which adopts a perturbed stationary state expansion of the molecular orbitals, to this collision system with the ultimate aim of extending the cross section down to threshold to provide data relevant for astrophysical modeling.

In this work, we explore the quenching and excitation processes



for energies between 0.001 eV and 10 eV. A brief description of the theoretical methods are presented in Sec. II. In Sec. III, the adiabatic potentials and nonadiabatic couplings of Na-He are discussed. The resulting cross sections and rate coefficients are given in Secs. IV A and IV B. Sections V and VI discuss astrophysical implications and summarize the work, respectively. Atomic units are employed unless otherwise stated.

II. THEORETICAL METHODS**A. Electronic structure calculations**

The *ab initio* adiabatic potentials and nonadiabatic couplings are obtained with the multireference single- and double-excitation configuration interaction (MRD-CI) method which has been detailed previously by Buenker and co-workers [12–17]. Here only descriptions relevant to the present calculation are specified. The basis functions for the molecular calculations consist of contracted Gaussian-type functions which have the form

$$N_n r^{n-1} e^{-\zeta r^2} Y_{lm}(\Omega), \quad (2)$$

where N_n is the normalization constant and Y_{lm} is a spherical harmonic. The (5s4p3d) basis for the helium atom [18] is contracted to [4s4p2d] including one *s*-, one *p*-, and one *d*-type diffuse functions with exponents which are 0.027, 0.023, and 0.020, respectively. For the sodium atom [19], the (15s9p5d) basis is contracted in [9s7p5d] including one *s*-, one *p*-, and one *d*-type diffuse functions with exponents which are 0.023, 0.021, and 0.018, respectively. The finite difference technique [20,21] has been applied to obtain radial couplings (matrix elements of $\partial/\partial R$), while rotational cou-

*chih-yuan.lin@obspm.fr

TABLE I. Parameters of long-range potentials for $1^2\Sigma^+$, $1^2\Pi$, and $2^2\Sigma^+$ corresponding to Eqs. (5) and (6) and comparison with other available predictions of dispersion coefficients. Also listed are the equilibrium distances r_m and well depths ϵ . All values are given in atomic units. The notation $A[B]=A \times 10^B$.

Molecular states	a	b	χ	C_6	C_8	C_{10}	r_m	ϵ
$1^2\Sigma^+$	4.35[3]	1.00	86.8	25.1 ^a	1.33[3]	9.51[4]	12.0	5.95[-6]
				24.10 ^b	1.249[3] ^b	8.8810[4] ^b		
				23.77 ^c	1.308[3] ^c	9.4563[4] ^c		
				25.76 ^d	1.329[3] ^d	9.7740[4] ^d		
$1^2\Pi$	5.18[2]	1.71	65.4	43.4 ^a	5.98[2]	1.07[4]	4.2	3.01[-3]
$2^2\Sigma^+$	8.40[3]	0.63	86.0	79.5 ^a	1.07[4]	1.86[6]	21.5	5.82[-7]

^aReference [27].

^bReference [28].

^cReference [29].

^dReference [31].

plings have been calculated by employing appropriate pairs of CI eigenfunctions. All couplings have been computed with the electronic coordinate origin at the center of mass of the Na-He system. The absolute CI energies are converged to 10^{-7} hartree.

B. Scattering theory

The quantum-mechanical MOCC approach, which has been described previously [22,23], is employed in the scattering calculations. Within the perturbed stationary state approximation, the basis wave functions are constructed from adiabatic molecular orbitals and electron translation factors are neglected. For given sets of basis functions, taking advantage of the variational principle leads to a set of coupled equations in the adiabatic representation. Employing the partial-wave expansion, a set of coupled radial equations is obtained. For numerical convenience, the coupled equations in the adiabatic representation are converted into a diabatic representation through a unitary transformation. The set of coupled second-order differential radial equations without first-order derivatives can then be solved by using the multichannel log-derivative method of Johnson [24]. From the numerical results and the analytical asymptotic expressions of the radial functions, the K matrix may be extracted and thus the S matrix is given by

$$S^J = [I - iK^J]^{-1}[I + iK^J], \quad (3)$$

where J is the total angular momentum and I is the identity matrix. The collisional cross sections from the channel α to the channel β are expressed in terms of the scattering matrix elements

$$\sigma_{\alpha \rightarrow \beta} = \frac{\pi g_\alpha}{k_\alpha^2} \sum_J (2J+1) |\delta_{\alpha\beta} - S_{\alpha\beta}^J|^2, \quad (4)$$

where k_α denotes the wave number for the center-of-mass motion of the initial incoming channel momentum, and g_α is the initial approach probability factor.

III. POTENTIALS AND COUPLINGS

For low-energy collisions of Na($3s, 3p$) with He, the major effects and interactions for this system are dominated by three molecular states, $1^2\Sigma^+$, $1^2\Pi$, and $2^2\Sigma^+$, and three couplings connecting them. For the present scattering calculations, we do not consider the spin-orbit splitting in Na($3p^2P_J^o$), which has a value of 17.20 cm^{-1} (2.13 meV), and therefore restrict the considered collision energies to above 1 meV/u. The adiabatic potentials for these states are fitted to long-range dispersion coefficients and adjusted with a model interaction in the van der Waals well region. We used *ab initio* data calculated with the MRD-CI method as a function of internuclear distance R from 0.2 to 9.5 a.u. For R greater than 9.5 a.u., the model potential proposed by Cvetko *et al.* [25],

$$U(R) = \frac{C_6}{120} \left(\frac{b}{3}\right)^6 (ae^{-bR} - \chi e^{-(2/3)bR} - e^{-(1/3)bR}), \quad bR \leq 16.6, \quad (5)$$

was used to join the van der Waals well region smoothly to the long-range part of the potentials, while the long-range potential is described by

$$U(R) = \frac{C_6}{120} \left(\frac{b}{3}\right)^6 ae^{-bR} - \frac{C_6}{R^6} - \frac{C_8}{R^8} - \frac{C_{10}}{R^{10}}, \quad bR \geq 16.6. \quad (6)$$

The fitted energies obtained by Eq. (5) are adopted for the range of R between 9.5 a.u. and 16.6 a.u. for $1^2\Sigma^+$, 9.71 a.u. for $1^2\Pi$, and 26.35 a.u. for $2^2\Sigma^+$. The discrepancies between the fitted and *ab initio* data are less than $\sim 10^{-5}$ hartree for $1^2\Sigma^+$ and $1^2\Pi$, and $\sim 10^{-4}$ hartree for $2^2\Sigma^+$. While the C_8 and C_{10} coefficients can be obtained utilizing the universal correlation [26] and the continuity between the short-range and long-range part of model potentials, Eq. (6) is used to extrapolate the potentials to the long-range part. The parameters adopted for each molecular state are listed in Table I, where the C_6 coefficients are taken from Zhu *et al.* [27] and the others are obtained by fitting to the *ab initio* data. We also present in Table I, the equilibrium separations r_m and

TABLE II. Comparison of asymptotic separated-atom energies between the MRD-CI calculations and experiment for the lowest three molecular states of Na-He.

Separated-atom states	Experimental energies (eV) ^a	Theoretical energies (eV)	Molecular states	United-atom states
Na($3s\ ^2S$)+He	0.0	0.0	$1\ ^2\Sigma^+$	Al($3p\ ^2P^o$)
Na($3p\ ^2P^o$)+He	2.1037	2.0768	$1\ ^2\Pi$	Al($3p\ ^2P^o$)
		2.0868	$2\ ^2\Sigma^+$	Al($4s\ ^2S$)

^aNIST Atomic Spectra Database, Ref.[39].

well depths ϵ obtained from our fits. Compared to other theoretical predictions of the dispersion coefficients [28–31], the C_6 , C_8 , and C_{10} that we utilize for the $1\ ^2\Sigma^+$ state are in a good agreement. We are unaware of other determinations of C_8 and C_{10} for the excited states. r_m and ϵ for the ground state are within 1% and 3%, respectively, of the values computed in Refs. [25,30]. While similar parameters have not been previously reported for the $2\ ^2\Sigma^+$, our r_m is within the uncertainty of the measurement of Havey, Frolking, and Wright [32]. However, our well depth is 38% larger than the experimental value [32]. As the internuclear distance approaches infinity, these three molecular states degenerate into two separated-atom states which are Na($3s\ ^2S$)+He and Na($3p\ ^2P^o$)+He as given in Table II.

A unitary transformation [33] is applied to transform the potentials and couplings into a diabatic representation. The adiabatic and diabatic potentials are displayed in Fig. 1. The

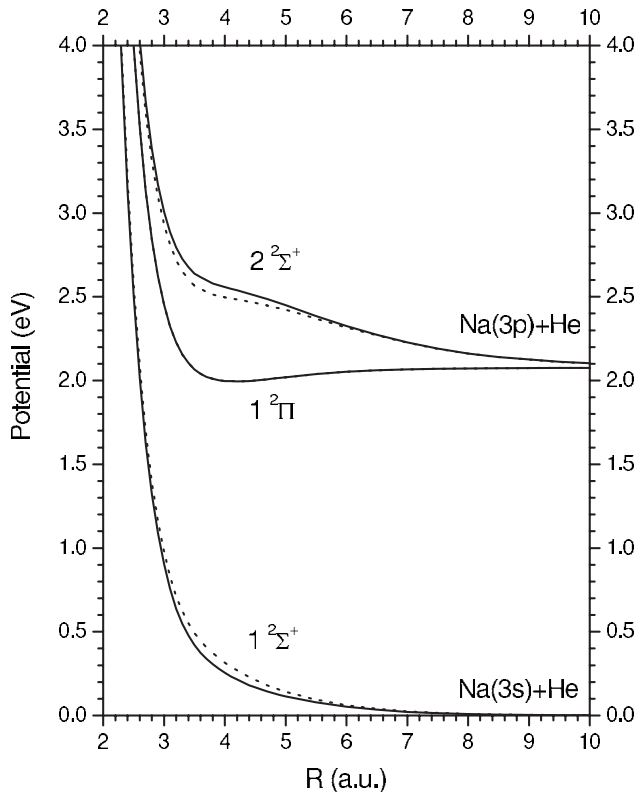


FIG. 1. Adiabatic (solid curves) and diabatic (dotted curves) potentials for Na-He as functions of internuclear distance R . The adiabatic and diabatic potentials for the $1\ ^2\Pi$ state are indistinguishable.

largest modifications due to the unitary transformation are for the $1\ ^2\Sigma^+$ and $2\ ^2\Sigma^+$ potentials. For couplings driving the transitions between different molecular states, there are two nonadiabatic rotational couplings, which result from the interaction between molecular states with different symmetry ($\Lambda = \Lambda' \pm 1$), and one nonadiabatic radial coupling, which is due to the interaction between molecular states with the same symmetry ($\Lambda = \Lambda'$). Λ is the projection quantum number of the electronic orbital angular momentum onto the internuclear axis. The nonadiabatic radial coupling element, which couples $1\ ^2\Sigma^+$ and $2\ ^2\Sigma^+$ via the operator $\partial/\partial R$, is presented in Fig. 2(a). In Fig. 2(b), we display two nonadiabatic rotational coupling elements, which couple the states $1\ ^2\Sigma^+$ and $2\ ^2\Sigma^+$ with $1\ ^2\Pi$ via the operator iL_y . L_y is the y component of the electronic angular momentum in the body-fixed frame. The diabatic coupling connecting the $1\ ^2\Sigma^+$ state with $2\ ^2\Sigma^+$ state is presented in Fig. 3(a), where the prime symbol stands for the diabatic states. Figure 3(b) shows the diabatic couplings which connect $2\ ^2\Sigma^+$ states with the $2\ ^2\Pi$ state.

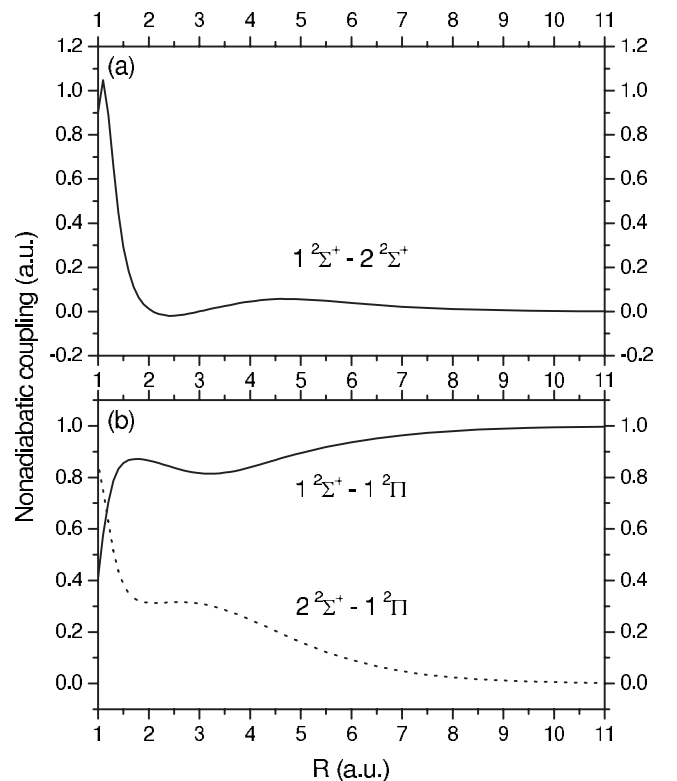


FIG. 2. The nonadiabatic radial coupling (a) and nonadiabatic rotational couplings (b) as functions of internuclear distance R .

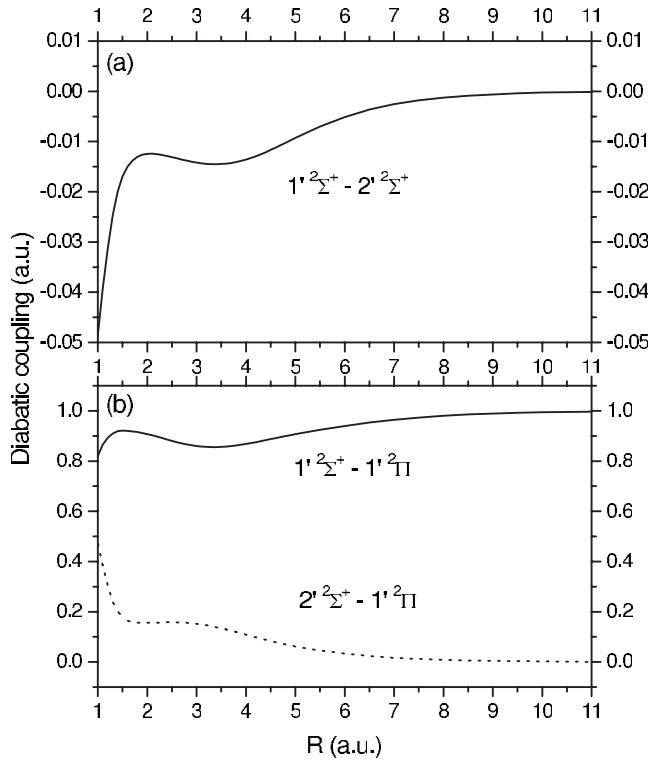


FIG. 3. Diabatic couplings for $2\Sigma^+$ state coupled with $2\Sigma^+$ state (a) and 2Π state (b) as functions of internuclear distance R .

IV. RESULTS AND DISCUSSION

A. Cross sections

The cross sections for inelastic collisions (1), which include quenching and excitation reactions, are displayed, respectively, in Fig. 4 and Fig. 5. The quenching process from $\text{Na}(3p)$ to $\text{Na}(3s)$ due to collisions of He includes two deexcitation paths, $1^2\Pi$ to $1^2\Sigma^+$ and $2^2\Sigma^+$ to $1^2\Sigma^+$. Figure 4

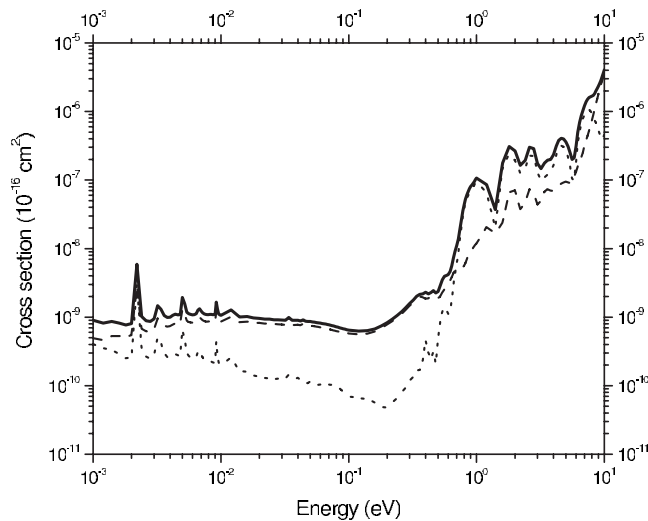


FIG. 4. The total (solid curve) and state-to-state quenching cross sections. The dashed curve corresponds to the deexcitation of molecular states from $1^2\Pi$ to $1^2\Sigma^+$ and dotted curve corresponds to that from $2^2\Sigma^+$ to $1^2\Sigma^+$.

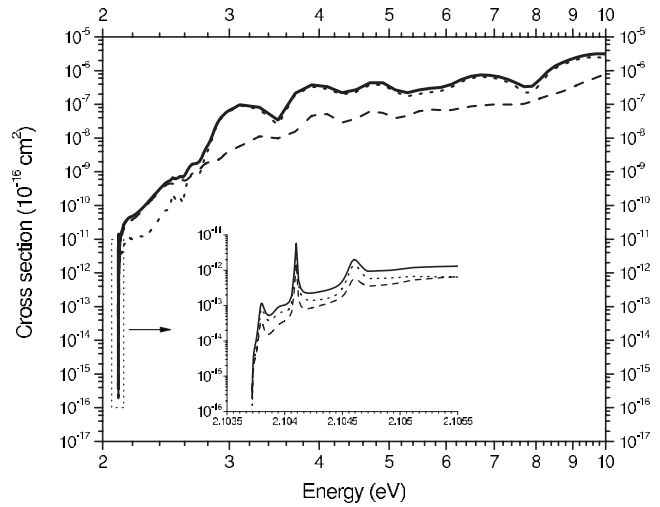


FIG. 5. The total (solid curve) and state-to-state excitation cross sections. The dashed curve corresponds to the excitation of molecular states from $1^2\Sigma^+$ to $1^2\Pi$ and dotted curve corresponds to that from $1^2\Sigma^+$ to $1^2\Sigma^+$. The inset shows the energy region near threshold.

displays the total and state-to-state cross sections. For energies less than 0.6 eV, quenching from $1^2\Pi$ to $1^2\Sigma^+$ is mostly the dominant process. On the contrary, quenching from $2^2\Sigma^+$ to $1^2\Sigma^+$ becomes more dominant as the energy increases, because the most significant coupling between $2^2\Sigma^+$ and $1^2\Sigma^+$ states occurs in the short range. Several distinct orbiting resonances appearing in the cross sections are due to quasibound states of the quasimolecule. It is worth noting that both different quenching processes have the same resonance position.

The excitation cross sections of $\text{Na}(3s)$ to $\text{Na}(3p)$ due to He collisions are given in Fig. 5. The most significant contribution to total excitation cross sections is through the excitation of molecular state $1^2\Sigma^+$ to $2^2\Sigma^+$ for energies larger than 2.8 eV. Because of the $2^2\Sigma^+$ threshold at 2.1 eV, the cross sections go to zero abruptly as the threshold is approached. The inset details the orbiting resonances occurring near the threshold.

The sensitivity of cross sections with respect to the variation of the potential energies depends on the collisional energy, particularly for low-energy collisions. In the present calculation, the influence of long-range potentials is explored by the variation of the C_6 , C_8 , and C_{10} coefficients. The cross sections for collision energies near 0.001 eV display differences less than 0.001% due to the change of C_6 up to 10% and have negligible variation due to the change of C_8 and C_{10} . While the variation of the reduced mass is equivalent to modifying the depth of the van der Waals well, varying the reduced mass up to 10% could cause an order of magnitude difference in cross sections for energies ~ 0.001 eV, but the discrepancies in the cross sections reduces to $\sim 20\%$ as the energy raises to ~ 0.1 eV. However, for collision energies less than 0.1 eV, the quenching cross sections are very small, typically less than $\sim 10^{-25}$ cm^2 , except near a resonance.

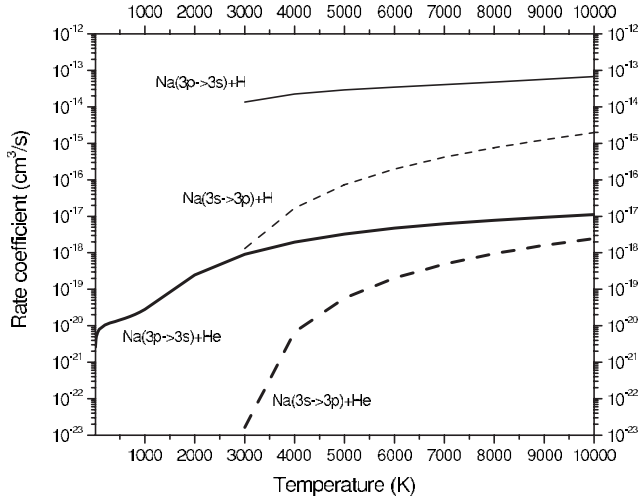


FIG. 6. Rate coefficients of inelastic collision processes, $\text{Na}(3p^2P^o)+X \rightarrow \text{Na}(3s^2S)+X$ (solid curve) and $\text{Na}(3s^2S)+X \rightarrow \text{Na}(3p^2P^o)+X$ (dashed curve), as functions of temperature T . Thick curves for $X=\text{He}$ and thin curves for $X=\text{H}$.

B. Rate coefficients

The rate coefficients $\alpha(T)$, where T is the temperature, are determined by averaging over the cross section $\sigma(E)$ with the Maxwellian energy distribution,

$$\alpha(T) = \frac{1}{\sqrt{\pi\mu}} \left(\frac{2}{kT} \right)^{3/2} \int_0^\infty \sigma(E) E \exp(-E/kT) dE, \quad (7)$$

where k is the Boltzmann constant and μ is the reduced mass of the system. Figure 6 illustrates the variation of the rate coefficients with T from 10 to 10^4 K for the quenching and excitation of Na due to collisions with He, which are compared to the same transitions of Na but due to collisions with H. The Na-H rate coefficients are obtained from the cross sections of Belyaev *et al.* [34]. Both Na-He and Na-H rate coefficients have similar behavior for quenching and excitation processes except for the obvious difference in their magnitudes. The rate coefficients are larger for the exoergic reaction, $\text{Na}(3p^2P^o)+\text{He} \rightarrow \text{Na}(3s^2S)+\text{He}$, than for the endoergic reaction, $\text{Na}(3s^2S)+\text{He} \rightarrow \text{Na}(3p^2P^o)+\text{He}$, as ex-

pected. For convenience we have fitted the inelastic rate coefficients to the relation

$$\alpha(T) = \sum_i a_i \left(\frac{T}{10\,000} \right)^{b_i} \exp\left(-\frac{T}{c_i}\right). \quad (8)$$

The fit coefficients of Na-He and Na-H collisions are given in Table III and are valid for $T < 10\,000\text{K}$. The rate coefficients themselves are reliable to within $\sim 20\%$, as indicated by our study of the variation of the cross sections with scaling of the potentials.

V. ASTROPHYSICAL IMPLICATIONS

The Na D line is observed in absorption in a variety of astrophysical sources and in emission when sufficiently energetic electrons are available to populate the $3p$ levels. In the former case, the density in most objects, e.g., stellar atmospheres, is large enough to ensure that the electronic levels are in local thermodynamic equilibrium (LTE).

While the indirect observation of atomic Na in the atmosphere of the transiting EGP HD 209458b was an important achievement [1], the observed difference in the transit depth in and out of the region of the Na D line was only about one-half that expected from model predictions [35–37]. A number of possibilities to explain this discrepancy was suggested by Charbonneau *et al.* [1] and later expanded on by Fortney *et al.* [38]. They considered the following scenarios: Depletion of Na into molecules and/or condensates, subsolar metallicity (though its companion star is of solar metallicity), non-LTE (NLTE) Na photoionization due to the companion's ultraviolet (uv) flux, and cloud opacity. Using a parametrized description of the cloud's vertical distribution and base, Fortney *et al.* were able to reproduce the observations as cloud opacity tends to reduce the strength of line absorption features. However, the physics of cloud formation is still in its infancy and a complete, robust description requires a treatment of gravitational settling of the condensate grains which is not yet available.

Barman *et al.* [2] proposed another possibility for which, in principle, the physics is well known: Na is in NLTE. This explanation has a number of attractive features: Exotic processes do not need to be imposed and Na (and other species) is likely to be in NLTE. This is the case due to the low

TABLE III. Fitting parameters of inelastic rate coefficients for $\text{Na}(3s \rightarrow 3p)$ excitation and $\text{Na}(3p \rightarrow 3s)$ quenching due to collisions with He and H. The notation $A[-B]=A \times 10^{-B}$.

	$\text{Na}(3s \rightarrow 3p)$		$\text{Na}(3p \rightarrow 3s)$	
	He (4000–10000 K)	H (3000–10000 K)	He (10–10000 K)	H (3000–10000 K)
a_1 (cm^3/s)	7.53[–12]	9.567[–12]	4.80[–20]	1.175[–12]
b_1	10.00	10.458	0.39	5.440
c_1 (K)	723.44	1097.773	2000.00	3341.270
a_2 (cm^3/s)	1.55[–9]	2.469[–9]	1.80[–16]	2.108[–11]
b_2	21.00	22.352	3.83	4.198
c_2 (K)	551.40	674.551	3500.00	1279.273

effective temperature of the planet (~ 1500 K), which results in low electron abundances ($\sim 10^{-8}$), and the strong, non-Planckian uv radiation from the primary which is only 0.045 AU away. The lack of electrons means that the Na level populations can only be thermalized by collisions with H_2 , He, or H which are expected to have smaller collisional cross sections. Unfortunately, the difficulty in performing NLTE calculations is the lack of collisional rate coefficients for the dominant atmospheric constituent H_2 . In their model, Barman *et al.* [2] used electron excitation rate coefficients as a substitute for H_2 rate coefficients and found significant departures in the $3s$ and $3p$ level populations from LTE. This resulted in a reversal in the core of the Na D absorption lines which would appear as a reduced line depth in low resolution.

In the current work, we have obtained rate coefficients for collisional excitation and deexcitation of Na due to He as shown in Fig. 6. The rate coefficients are very small for temperatures less than 10^4 K and will therefore be very inefficient at thermalizing the Na level populations. In Fig. 6, the Na-He rate coefficients are compared to the same transitions for collisions due to H. While the Na-H rate coefficients are 4–5 orders of magnitude larger, atomic hydrogen will mostly be tied up in H_2 in an EGP, so that the relative efficiency of the Na-H to Na-He processes will be significantly smaller than the ratio of the rate coefficients. The excitation rate coefficients for collisions due to H_2 are currently unknown, but their magnitude might be expected to be intermediate between the H and He perturber values. As the rate coefficients for all neutral perturbers are smaller than those due to electron impact, the significant departure from

LTE obtained by Barman *et al.* would appear to be a robust result and a valid interpretation for a inferred reduced Na abundance in HD 209458b.

VI. SUMMARY

Inelastic collisions of Na($3s, 3p$) with He have been investigated using the quantum-mechanical MOCC approach. The results include total cross sections, state-to-state cross sections, and rate coefficients for the quenching and excitation processes (1). The quenching cross sections in the low-energy region are dominated mostly by the deexcitation from $1^2\Pi$ to $1^2\Sigma^+$. The coupling between $1^2\Sigma^+$ and $2^2\Sigma^+$ states results in the transitions between $1^2\Sigma^+$ and $2^2\Sigma^+$ states becoming more dominant in the high-energy region. The small rate coefficients obtained for inelastic collisions of Na with He strengthens the argument made by Barman *et al.* [2] that the sodium electronic level populations are out of equilibrium in the atmosphere of the extrasolar giant planet HD 209458b.

ACKNOWLEDGMENTS

C.Y.L. and P.C.S. acknowledge support from NASA Grant No. NNG04GM59G. R.J.B. acknowledges the financial support of Grant No. Bu 450/7-3 from the Deutsche Forschungsgemeinschaft. We thank Dr. Belyaev for providing his Na-H cross sections in numerical form. P.C.S. thanks Peter Hauschildt and Travis Barman for discussions on extrasolar planet applications.

-
- [1] D. Charbonneau, T. M. Brown, R. W. Noyes, and R. L. Gilliland, *Astrophys. J.* **568**, 377 (2002).
 - [2] T. S. Barman, P. H. Hauschildt, A. Schweitzer, P. C. Stancil, E. Baron, and F. Allard, *Astrophys. J.* **569**, L51 (2002).
 - [3] C. Bottcher, T. C. Cravens, and A. Dalgarno, *Proc. R. Soc. London, Ser. A* **346**, 157 (1975).
 - [4] N. Andersen and S. E. Nielsen, *Advanced Atomic Molecular Physics* (Academic, New York, 1982), Vol. 18, p. 265.
 - [5] C. Courbin-Gaussorgues and V. Sidis, *J. Phys. B* **18**, 699 (1985).
 - [6] M. Kimura and J. Pascale, *J. Phys. B* **18**, 2719 (1985).
 - [7] W. Mecklenbrauck, J. Schön, E. Speller, and V. Kempter, *J. Phys. B* **10**, 3271 (1977).
 - [8] J. O. Olsen, N. Andersen, and T. Andersen, *J. Phys. B* **10**, 1723 (1977).
 - [9] N. Andersen, T. Andersen, K. Bahr, C. L. Coche, E. H. Pedersen, and J. O. Olsen, *J. Phys. B* **12**, 2529 (1979).
 - [10] L. L. Vahala, P. S. Julienne, and M. D. Havey, *Phys. Rev. A* **34**, 1856 (1986).
 - [11] C. Zhu, J. F. Babb, and A. Dalgarno, *Phys. Rev. A* **73**, 012506 (2006).
 - [12] R. J. Buenker and S. D. Peyerimhoff, *Theor. Chim. Acta* **35**, 33 (1974).
 - [13] R. J. Buenker and S. D. Peyerimhoff, *Theor. Chim. Acta* **39**, 217 (1975).
 - [14] R. J. Buenker, in *Proceedings of the Workshop on Quantum Chemistry and Molecular Physics*, edited by P. G. Burton (University of Wollongong Press, Wollongong, Australia, 1980), p. 1.5.1.
 - [15] R. J. Buenker, in *Current Aspects of Quantum Chemistry*, edited by R. Carbo (Elsevier, Amsterdam, 1982), Vol. 21, p. 17.
 - [16] R. J. Buenker and R. A. Philips, *J. Mol. Struct.: THEOCHEM* **123**, 291 (1985).
 - [17] S. Krebs and R. J. Buenker, *J. Chem. Phys.* **103**, 5613 (1995).
 - [18] D. E. Woon and J. T. H. Dunning, *J. Chem. Phys.* **100**, 2975 (1994).
 - [19] J. T. H. Dunning, *J. Chem. Phys.* **90**, 1007 (1989).
 - [20] C. Galloy and J. C. Lorquet, *J. Chem. Phys.* **67**, 4672 (1977).
 - [21] G. Hirsch, P. J. Bruna, R. J. Buenker, and S. D. Peyerimhoff, *J. Chem. Phys.* **45**, 335 (1980).
 - [22] B. Zygelman, D. L. Cooper, M. J. Ford, A. Dalgarno, J. Gerratt, and M. Raimondi, *Phys. Rev. A* **46**, 3846 (1992).
 - [23] B. Zygelman, P. C. Stancil, N. J. Clarke, and D. L. Cooper, *Phys. Rev. A* **56**, 457 (1997).
 - [24] B. R. Johnson, *J. Comput. Phys.* **13**, 445 (1973).
 - [25] D. Cvetko, A. Lausi, A. Morgante, F. Tommasini, P. Cortona, and M. G. Dondi, *J. Chem. Phys.* **100**, 2052 (1994).
 - [26] I. Borges, Jr., P. J. S. B. Caridade, and A. J. C. Varandas, *J. Mol. Spectrosc.* **209**, 24 (2001).
 - [27] C. Zhu, A. Dalgarno, S. G. Porsev, and A. Dereviako, *Phys.*

- Rev. A **70**, 032722 (2004).
- [28] T. R. Proctor and W. C. Stwalley, *J. Chem. Phys.* **66**, 2063 (1977).
- [29] U. Kleinekathöfer, K. T. Tang, J. P. Toennies, and C. L. Yiu, *Chem. Phys. Lett.* **249**, 257 (1996).
- [30] U. Kleinekathöfer, M. Lewerenz, and M. Mladenović, *Phys. Rev. Lett.* **83**, 4717 (1999).
- [31] J. Mitroy and M. W. J. Bromley, *Phys. Rev. A* **68**, 062710 (2003).
- [32] M. D. Havey, S. E. Frolking, and J. J. Wright, *Phys. Rev. Lett.* **45**, 1783 (1980).
- [33] T. G. Heil, S. E. Butler, and A. Dalgarno, *Phys. Rev. A* **23**, 1100 (1981).
- [34] A. K. Belyaev, J. Grosser, J. Hahne, and T. Menzel, *Phys. Rev. A* **60**, 2151 (1999).
- [35] S. Seager and D. D. Sasslov, *Astrophys. J.* **537**, 916 (2000).
- [36] T. M. Brown, D. Charbonneau, R. L. Gilliland, R. W. Noyes, and A. Burrows, *Astrophys. J.* **552**, 699 (2001).
- [37] W. B. Hubbard, J. J. Fortney, J. I. Lunine, A. Burrows, D. Sudarsky, and P. Pinto, *Astrophys. J.* **560**, 413 (2001).
- [38] J. J. Fortney, D. Sudarsky, I. Hubeny, C. S. Cooper, W. B. Hubbard, A. Burrows, and J. I. Lunine, *Astrophys. J.* **589**, 615 (2003).
- [39] <http://physics.nist.gov/asd3>